Difference between Korean and Occidental Group-specific Label-based Probabilistic Brain Atlas

구방본·이종민 (한양대학교)

I. Abstract

Probabilistic atlases for the human brain structure are more suitable than single brain atlases for representing population anatomy. In this study, we hypothesized the group-specific probabilistic atlas for accurate characteristic feature coding. Our proposed method for a new group comparison study, using a subpopulation specific probabilistic atlas, was based on this hypothesis. A knowledge-based automatic labeling technique using nonlinear registration was applied to encode group-specific regional probabilistic information. Direct atlas-based comparison using volume counting above the probability threshold, distance measurement and correlation analysis were performed based on the probabilistic atlas. Here, we applied this method for comparison between Korean and occidental groups. The results showed that this method could provide simple but intuitive regions of interest-based group analysis for the entire cortex area.

II. Introduction

The structure of the human brain is complex, with wide variations between individuals. These variations create fundamental problems in any group study and have stimulated the development of mathematical algorithms and atlases that compare, pool, and average across populations. Voxel-based and region-based methods are widely used to characterize variations in the structure and neuroanatomical configuration of different brains. For the voxel-based method, individual datasets are spatially transformed to a template in stereotaxic space, and statistical tests are applied to these spatially transformed images [Ashburner and Friston, 1997].

Since a single brain template may not be representative of the average anatomy, determining the exact anatomical localization is difficult. Region-based methods have been based on the *a priori* definition of a number of regions of interest (ROIs). In practice, it is not known in advance which regions might be affected by disease. The affected region might be only part of a well-characterized anatomical region, such as hippocampus, or it might span different regions. Although the prior information needs to be guaranteed, the region-based method provides more precise analysis. Another weak point is that this approach is extremely laborious. It requires the manual definition of many ROIs in a large number of subjects. To overcome this time-consuming problem, a standard anatomical template makes it feasible to define the multiple ROIs and can improve consistency of the outlining [Bajcsy et al., 1983; Bohm et al., 1991; Evans et al., 1988, 1992; Greitz et al., 1991; Kosugi et al., 1993; Christensen et al., 1997; Collins et al., 1999].

Another promising approach for characterizing information on group variability is a probabilistic atlas (Statistical Probability Anatomy Map: SPAM) [Evans et al., 1994]. The basic idea is to gather large ensembles of brain data from a homogeneous group and segment the data into sub-volumes after transforming each dataset into stereotaxic space. A probability map can be constructed for each segmented structure by determining the proportion of subjects assigned to a given anatomic label at each voxel position in stereotaxic space. The use of anatomical information in such probabilistic maps provides a measure of variability, in the location and the extent, of specific segmented areas among the subjects. It allows the statistical assessment of the normal ranges for both the structure and spatial extents in native and stereotaxic space.

Here, we hypothesized that a group-specific—i.e., ethnic, gender, age, or disease—probabilistic atlas would show differences that could reflect the characteristics of the group. Based on this hypothesis, we constructed a group comparison method using probabilistic atlases of each different group. However, few studies based on comparing probabilistic information on brain structure from different subpopulations have been made [Thompson et al., 2000]. We introduce a direct atlas-to-atlas comparison method using a labeled volume-based probabilistic atlas. A Korean probabilistic brain atlas, which was a labeled volume-based probabilistic atlas for a volumetric study of the neuroanatomical structures, was constructed and compared with the probabilistic atlas of the Montreal Neurological Institute (MNI). Common segmented areas were compared quantitatively in terms of the volume and distribution.

The aims of this study were: (1) to construct a group-specific probabilistic atlas and (2) to present a new group comparison method for its application.

III. MATERIALS AND METHODS

In this section, we describe the detailed construction procedure of a probabilistic atlas for a normal Korean population. The new comparison method is then described along with its application to a group study between Korean and occidental groups. In this case, a probabilistic atlas from MNI was used to represent the occidental group.

## 1. Construction of Korean Probabilistic Atlas

A label-based probabilistic atlas was constructed for a normal Korean group. The basic idea was to gather large ensembles of brain data from a homogeneous group and to segment them into sub-volumes after transforming each dataset into stereotaxic space. A probability map was then constructed for each segmented structure by determining the proportion of subjects assigned to a given anatomic label at each voxel position in stereotaxic space. The details of the construction procedure are described below.

1.1 Data Acquisition

The T1-weighted MR images of 76 healthy volunteers (50 men, 26 women) were acquired from the Department of Psychiatry and Nuclear Medicine, Seoul National University Hospital. The ages of the participants were normally distributed (mean age = 45.56±19.68 years). Magnetic resonance imaging was performed on a 1.5T GE SIGNA scanner (GE Medical System, Milwaukee, USA) using a 3D-SPGR T1-weighted spoiled gradient echo pulse sequence using the following parameters: 1.5 mm sagittal slices; echo time = 5.5 ms; repetition time = 14.4 ms; number of excitations = 1; rotation angle = 20° field of view = 21 × 21 cm; matrix = 256 × 256 mm. To improve the signal-to-noise ratio, the images were resampled to 1.0 mm^3 voxels and filtered using anisotropic diffusion methods. These procedures were processed using the commercial software ANALYZE 3.0 (Mayo Foundation, USA). The cerebrospinal fluid (CSF) and skull structure, which were not ROIs in the brain analysis, were removed using a conventional region-growing method that followed morphological procedures such as dilation and erosion. Tissue classification of the structure of gray matter and white matter were automatically classified [Yoon et al., 2003].

1.2 Standard Brain Construction and Spatial Normalization of the Data

A standard brain provides an appropriate common coordinate system and representative anatomical information. First, we selected a standard brain from the group using an automatic algorithm that searched for a brain containing the average properties in the Talairach coordinate system[Talairach et al., 1998]. This algorithm selected a single brain among the group by measuring 11 line-lengths of each data, which is based on the most anterior point-anterior commissure (AC); the most posterior point-posterior commissure (PC); the AC-PC line, which passes through the superior edge of
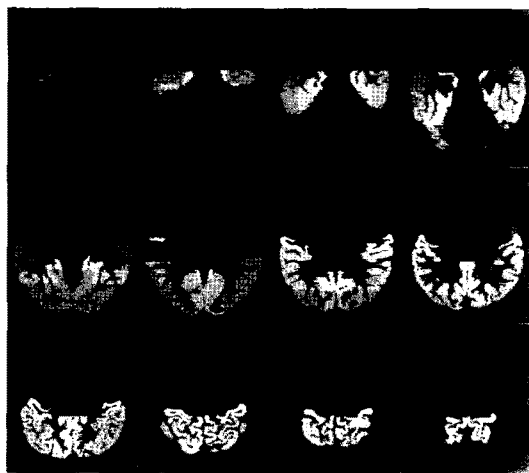
⟨Figure 1⟩ A color-coded image of the labeled template. Eighty-nine regions of interest were defined by manual drawing in the two-dimensional section and reconstructed into a three-dimensional volume image. Each three-dimensional volume was classified by a different color value

the AC and the inferior edge of the PC; the AC/PC-upper/lower vertical boundary in the sagittal direction; the AC left/right horizontal boundary; and the PC left/right horizontal boundary in the coronal direction [Lee et al., 2003]. A single brain, which had 11 line lengths close to the group average, was selected to be an initial representative brain. After this single brain selection, each 12 parameter affine transformations from all subjects to the single representative brain were derived [Kim et al., 2002]. These transformations were averaged to define a 'least distant space' for each subject to be transformed into. The data was then transformed into the common space using average transform parameters and an intensity average was performed to construct an average template. All the subjects were realigned with affine transformations to the average template and again averaged to form a linearly defined atlas in both intensity and spatial domains. Finally, all the data were transformed into a linear average atlas using a nonlinear registration method, and averaged to construct a nonlinear average atlas. After the nonlinear average atlas was constructed, all the data were spatially normalized into the atlas using nonlinear transformations [Kim et al., 2003].

1.3 Manual Segmentation

Manual segmentation was performed on

the initial representative brain described above. Eighty-nine ROIswere manually delineated for each 1 mm two-dimensional slice of the selected single brain using ANALYZE (version 3.0). These 89 ROIs were converted into three-dimensional volume images with a different gray-level code (0 to 89) and merged into the standard space <Fig. 1> The topographic uniqueness of the individual cerebral cortex was preserved and the strengths of the two-dimensional and three-dimensional visualization were relied on to identify cerebral landmarks and conduct measurements with the information from the three orthogonal planes (transaxial, coronal and sagittal) and the three-dimensional rendered brain. The detailed architectonic profiles of the ROIswere defined on the brain template for macro-level anatomical labels. Seventy-five ROIs were described in previous studies [Crespo-Facorro et al., 1999, 2000; Kim et al., 2000].

1.4 Automatic Labeling and
.   Probabilistic Encoding

Although manually delineating the ROIs for all data appears to be more reasonable for making a real probability, it is a very time-consuming process to segment all data. To deal with this problem, only automated labeling methods were used to transform the three-dimensional ROIs template images into each subject. The nonlinear transformation required us to customize the labeled template, which, manually defined above, was estimated by our locally developed algorithm [Kim et al., 2003], and preprocessed tissue data were used for classification error correction. The variability of each local structure was then described in a probability by counting the occurrence of each ROI at the voxel levelacross the 76 datasets, and the occurrence of each ROI was encoded by a gray value.

As the automatic labeling procedure was mostly influenced by the registration procedure, we defined 18 landmarks that could be readily identified on each brain to evaluate the accuracy of the automatic labeling procedure. This was based on the idea that all spatially transformed templates should occupy the same space as the individual MR images, and therefore landmarks within these images should be very close to each other. The landmarks were uniformly distributed over the whole brain and identified manually using a cursor. The landmarks on the standard brain template were transformed to each brain space using nonlinear transformation and compared with each corresponding landmark that was manually identified in each subject's image in order to yield the

average Euclidean distance.

2. Group Comparison Study Using Probabilistic Atlases

We constructed three comparison factors for the group comparison method using subpopulation-specific probabilistic atlases. The three factors were probabilistic volume counting above the thresholds, probabilistic center-of-mass and distance measure and correlation coefficient of each corresponding ROI. The details of these factors are described in subsections below. These three factors were applied to compare Korean and occidental groups. Early efforts to construct an MNI probabilistic atlas were documented by Evans and colleagues [Evans et al. 1994].

2.1 Standard Space Matching

The initial step in the intergroup analysis using the group-specific probabilistic atlas was the template-matching step. A nonlinear transformation from the average space of the Korean probability atlas into MNI stereotaxic space, which was constructed from the intensity average of 305 MR image volumes [Evans et al. 1992], was obtained. The Korean probabilistic atlas was then transformed and resampled by applying the nonlinear transformation.

2.2 ROI Matching

The corresponding ROIs between the two atlases were extracted by neuroanatomically trained investigators (KJJ, LDS, KEJ).The delineation algorithms of the two probabilistic atlases were evaluated for constructing the correspondence of each ROI. The definition of each border of the ROIs, such as anterior, posterior, medial, lateral, superior and inferior borders, and anatomical landmarks, were used for evaluation. The delineation algorithms for constructing the MNI probabilistic atlas were reported by Kabani [Kabani, 1998]. As the number of defined ROIs in the MNI probabilistic atlas was more than the number of ROIs defined in our method, the ROIs for undefined areas in the Korean probabilistic atlas, such as white matter, cerebrospinal fluid, dura mater, ventricle and scalp structures, were initially excluded from the matching procedure. Then, the remaining 75 ROIs in the MNI probabilistic atlas were used to match with the 89 ROIs in the Korean probabilistic atlas. As there was not an exact one-to-one match for all cases, several ROIs could be matched with a single ROI, or the converse

2.3 Difference Evaluation

After the ROI matching procedure was performed, the three factors were used to

compare the corresponding structures.

(1) Probabilistic volume counting above the thresholds

When x_i is a voxel in the i-th ROI and $p(x_i)$ is a probability of x_i, a probabilistic volume counting of j-th ROI(V_{Sj}) is defined as

$$Vs_j(\tau) = \sum_i G(p(x_i)) \tag{1}$$

$G(p(x_i))$ is the converting function. If $p(x_i)$ is above the threshold(τ), $G(p(x_i))$ has the value '1', otherwise '0'. In this study, we changed τ in the range from 0 to 1 by 0.25 for probabilistic volume measure. Then, we defined the degree of variability as $Vs_j(0.5)/Vs_j(0)$. A lower degree of variability value indicates a higher degree of variability.

(2) Probabilistic center-of-mass and distance measure

A probabilistic center of mass for each ROI is defined as

$$X_{CM} = [\frac{\sum_i p_i x_i}{\sum_i p_i}, \frac{\sum_i p_i y_i}{\sum_i p_i}, \frac{\sum_i p_i z_i}{\sum_i p_i}] \tag{2}$$

Here, x_i, y_i, z_i is a coordinate of the i-th voxel and p_i is a probability value of the i-th voxel. After the calculation of a probabilistic center of mass in both corresponding ROIs, the Euclidian distance between each center of mass of each ROI was calculated in order to assess the spatial locating difference of two matched regions in stereotaxic space.

(3) Correlation coefficient of each corresponding ROI

The correlation coefficient is defined as

$$CC = \frac{N\sum_{i,j,k} p(a_{ijk})p(b_{ijk}) - (\sum_{i,j,k} p(a_{ijk}))(\sum_{i,j,k} p(b_{ijk}))}{\sqrt{[N\sum_{i,j,k} p^2(a_{ijk}) - (\sum_{i,j,k} p(a_{ijk}))^2][N\sum_{i,j,k} p^2(a_{ijk}) - (\sum_{i,j,k} p(a_{ijk}))^2]}}$$
$$i, j, k \in (S1 \cup S2) \tag{3}$$

where N denotes the number of voxels in the ROI and a_{ijk}, b_{ijk} are voxels in corresponding ROIs $(S1, S2)$. Note that voxels that have no probabilistic value in both ROIs are not used for computing the correlation coefficients.

IV. Results

1. Construction of a Korean Probabilistic Atlas

1.1 Standard brain construction

The boundary box size of the constructed average atlas was 16.8 x 15.1 x 14.0 cm. The average size of the group was 16.3 x 15.4 x 14.2 cm and the MNI 305 template was 19.0 x 15.7 x 13.4 cm. The gray

⟨Table 1⟩ Volume comparison of astandard brain template

(cc)	Korean standard	MNI standard	MNI averaged 305
Gray Matter	809.28	1057.89	1001.92
White Matter	531.39	780.43	673.35
CSF	46.02	60.37	54.75

matter, white matter, and CSF tissue volumes of selected individual standard brains were less than the MNI standard individual brain, which was used for manual delineation, and also less than the MNI average 305 brain templates ⟨Table 1⟩.

1.2 Evaluation of nonlinear registration used in automatic labeling procedure

As explained under Methods, we evaluated the accuracy of our registration algorithm. Euclidean distances between 18 transformed points and manually defined points, which were defined in the target image,are shown in ⟨Table 2⟩. The assessment of the spatial transformation process yielded an average Euclidean distance of 1.83 ± 1.55. Some landmarks were associated with smaller variability than others e.g., the posterior tip of the 4th ventricle landmark only had 1.12 mm average distance, whereas the anterior end of the right parieto-occipital sulcus landmark had 2.67 mm average distance.

1.3 Comparison between Korean and MNI Probabilistic Atlases

The final ROI matching procedure was successfully applied, except for some regions: the left/right precuneus, the left/right medial fronto-orbital gyrus, and the left/right cingulate gyrus. The volume differences of these ROIs exceeded 50% in these regions. These results showed that biased results could be induced in probabilistic volume counting ⟨Fig 2⟩. In the standard space-matching step, the algorithm was successfully applied in the procedure. The results for difference evaluations are given in ⟨Table 3⟩ The average of correlation coefficients for 46 matched regions was 0.41. In the point of average correlation coefficients for each lobe, ROIs in the temporal lobe (0.34) and parietal lobe (0.24) showed lower values in comparison to other lobes. In these lobes, the degree of variability in the Korean probabilistic template was much larger than in the MNI template, especially in the left middle temporal gyrus (Korean: 0.25, MNI: 0.36), and the left/right postcentral gyrus (left—Korean: 0.21, MNI: 0.3; right—Korean: 0.12, MNI: 0.38). The opposite was observed in the right superior temporal gyrus (Korean: 0.28, MNI: 0.2) and the left/right supra-marginal gyrus (left—Korean: 0.28, MNI: 0.1; right—Korean: 0.64, MNI: 0.2). The ROIs in the occipital

〈Table 2〉 Labeling error estimation using 18 landmarks

Point Landmarks	Average Distance	Standard Deviation
In the midline sagittal slice		
1. AC (Anterior Commissure)	1.67	0.83
2. PC (Posterior Commissure)	1.76	0.93
3. Anterior tip of the corpus callosum	1.82	1.25
4. Posterior tip of the corpus callosum	1.79	1.10
5. Posterior tip of the 4th ventricle	1.12	1.19
6. Posterior end of the cerebellum at the level of 5	2.39	1.37
7. Inferior notch of the pons	0.27	1.52
In the sagittal slice of (midline − 5)		
8. Anterior tip of the right cingulated sulcus at the level of 3	1.97	1.10
9. Posterior end of the right cingulated sulcus	2.16	1.47
10. Anterior end of the right parietooccipital sulcus	1.67	2.08
11. Posterior end of the right parietooccipital sulcus	2.17	1.64
In the sagittal slice of (midline + 5)		
12. Anterior tip of the left cingulated sulcus at the level of 3	2.29	1.62
13. Posterior end of the left cingulated sulcus	2.34	1.57
14. Anterior end of the left parietooccipital sulcus	2.67	1.92
15. Posterior end of the left parietooccipital sulcus	2.39	2.23
In the transverse slice at the level of AC/PC		
16. Right posterior end of the sylvian fissure (or insula)	1.37	1.22
17. Left posterior end of the sylvian fissure (or insula)	1.62	1.61
In the transverse slice at the level of 3		
18. Anterior end of the right lateral ventricle	1.47	1.31
Average	1.83	1.55

Number	Region of Interest
1	Amygdala gyrus
2	Hippocampal Formation
3	Inf. Temporal gyrus
4	Mid. Temporal gyrus
5	Parahippocampal gyrus
6	Sup. Temporal gyrus
7	Postcentral gyrus
8	Supramarginal gyrus
9	Sup. Parietal lobe
10	Cuneus
11	Lingual gyrus
12	Precuneus
13	inf. Occipital gyrus
14	lat. OccipitoTemporal gyrus
15	Insula
16	Mid. Frontal gyrus
17	Sup. Frontal gyrus
18	med. FrontoOrbital gyrus
19	caudate nucleus
20	Globus Pallidus
21	Putamen
22	Cingulate
23	Thalamus
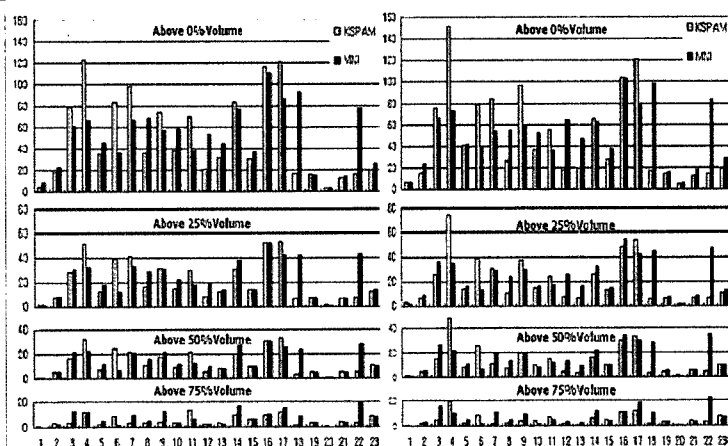
〈Figure 2〉 Probabilistic atlas comparison study. Subtracted volumes of the probability threshold from 1 to 0 by 0.25 were measured in each ROI for the left hemisphere (a) and the right hemisphere (b). Note that the y-axis indicates the volume [cc]. The blue color indicates the value of the Korean subjects and the red indicates that for the MNI. The number in the x-axis indicates the ROIs,which are listed in (c)

〈Table 3〉 a. In some cases, several ROIs in the Korean atlas were merged into one ROI in the MNI SPAM (a). Note that there was no case for merging several ROIs in the MNI SPAM into one ROI in the Korean atlas. Several ROIs are defined in each atlas (b)
b. Several ROIs are defined in each atlas (b)

(a)		(b)	
MNI	Korean	Defined only in the MNI SPAM	Defined only in the Korean atlas
Inferior Temporal Gyrus (ITG)	ITG, rostral ITG, intermediate ITG, caudal	Brain Stem Frontal Lobe White Matter Mid. Occipital Gyrus Nucleus Accumbens Septi Occipital Lobe White Matter Occipital Pole Subthalamic Nucleus Temporal Lobe White Matter Uncus 3rd Ventricle 4th Ventricle White Matter Anterior Limb of Internal Capsule Dura Matter Fornix Lateral Ventricle Post. Limb of Internal Capsule CSF/Scalp/Skull	Vermis Cerebelli
Mid. Temporal Gyrus (MTG)	MTG, rostral MTG, intermediate MTG, caudal		
Parahippocampal Gyrus (PHG)	PHG, rostral PHG, caudal		
Superior Temporal Gyrus (STG)	STG, rostral STG, caudal Temporal pole Heschl's Gyrus Planum polare Planum temporale		
Cingulate	Anterior Cingulate, caudal Anterior Cingulate, rostral Posterior Cingulate		
Lingual Gyrus Medial Occipitotemporal Gyrus	Lingual Gyrus		
Superior Frontal Gyrus Medial Frontal Gyrus	Superior Frontal Gyrus SMA		
Lateral Occipitotemporal gyrus (OTG)	OTG, rostral OTG, caudal Fusiform Gyrus		
Medial Orbitofrontal Gyrus Lateral Orbitofrontal Gyrus	Orbitofrontal Gyrus		

lobe and inner structures, such as the caudate nucleus, thalamus and putamen, showed high correlation coefficients except for some regions: left/right precuneus (left: 0.216, right: 0.161), left/right superior frontal gyrus (left: 0.3, right: 0.2), left/ rightmedial fronto-orbital gyrus (left: 0.227, right: 0.218) and left/right cingulate gyrus (left: 0.168, right: 0.184). Correlation coefficient values were highly influenced by large location differences, especially in both left and right superior frontal gyrus.

〈Table 4〉 Differences in the center, degree of variability and the correlation of the corresponding volume of each ROI. DOV = degree of variability; CC = correlation coefficient

	Matching ROI	Korean				MNI				Dist.	CC
		Center of Volume			DOV	Center of Volume			DOV		
		x	y	z		x	y	z			
Temporal	1.left Amygdala gyrus	−25	−10	−18	0.29	−27	−11	−22	0.33	4.58	0.495
	right Amygdala gyrus	23	−8	−18	0.38	23	−5	−21	0.29	4.24	0.561
	2.left Hippocampal Formation	−29	−24	−14	0.27	−33	−27	−17	0.21	5.83	0.426
	right Hippocampal Formation	27	−23	−13	0.32	27	−20	−16	0.20	4.24	0.595
	3.left Inf. Temporal gyrus	−56	−45	−21	0.21	−58	−37	.−26	0.35	9.64	0.307
	right Inf. Temporal gyrus	46	−38	−30	0.22	56	−39	−21	0.37	13.49	0.207
	4.left Mid. Temporal gyrus	−50	−47	−5	0.25	−66	−31	−8	0.36	22.82	0.284
	right Mid. Temporal gyrus	48	−41	−7	0.30	65	−22	−13	0.29	26.19	0.228
	5.left Parahippocampal gyrus	−22	−43	−9	0.20	−26	−34	−21	0.22	15.52	0.186
	right Parahippocampal gyrus	13	−48	−2	0.20	22	−25	−22	0.23	31.78	0.395
	6.left Sup. Temporal gyrus	−53	−21	0	0.30	−65	−24	0	0.28	12.36	0.167
	right Sup. Temporal gyrus	49	−11	−5	0.28	67	−14	0	0.20	18.92	0.218
Parietal	7.left Postcentral gyrus	−49	−23	20	0.21	−45	−32	65	0.30	46.07	0.194
	right Postcentral gyrus	61	−17	31	0.12	49	−24	59	0.38	31.26	0.290
	8.left Supramarginal gyrus	−56	−40	26	0.28	−52	−32	24	0.10	8.31	0.310
	right Supramarginal gyrus	55	−28	26	0.64	61	−31	29	0.20	9.27	0.280
	9.left Sup. Parietal lobe	−5	−63	51	0.25	−25	−67	68	0.37	26.55	0.185
	right Sup. Parietal lobe	4	−57	50	0.21	26	−62	67	0.34	28.25	0.193
Occipital	10.left Cuneus	−9	−83	19	0.22	−16	−75	26	0.17	12.72	0.404
	right Cuneus	5	−88	18	0.27	0	−83	14	0.18	8.12	0.444
	11.left Lingual gyrus	−13	−82	−2	0.29	−8	−74	−1	0.33	9.49	0.552
	right Lingual gyrus	6	−78	0	0.30	12	−66	−2	0.34	13.56	0.592
	12.left Precuneus	−5	−70	31	0.23	−7	−69	56	0.19	25.09	0.216
	right Precuneus	1	−65	31	0.22	1	−74	38	0.17	11.40	0.161
	13.left Inf. Occipital gyrus	−47	−88	7	0.28	−50	−83	−7	0.20	15.16	0.504
	right inf. Occipital gyrus	38	−94	2	0.14	39	−80	−6	0.20	16.15	0.412
	14.left lat. Occipitotemporal gyrus	−37	−46	−18	0.23	−36	−60	−16	0.30	14.18	0.453
	right lat. Occipitotemporal gyrus	33	−53	−14	0.26	34	−54	−16	0.35	2.45	0.468
Frontal	15.left Insula	−40	−3	3	0.32	−39	−3	−1	0.26	4.12	0.634
	right Insula	37	0	0	0.36	37	3	2	0.25	3.61	0.679
	16.left Mid. Frontal gyrus	−36	26	35	0.26	−34	36	28	0.28	12.36	0.421
	right Mid. Frontal gyrus	33	33	32	0.29	24	51	17	0.34	25.09	0.539
	17.left Sup. Frontal gyrus	−5	−2	58	0.26	−17	40	54	0.29	43.86	0.3
	right Sup. Frontal gyrus	3	14	62	0.27	6	33	58	0.36	33.38	0.2
	18.left med. Fronto-orbital gyrus	−5	30	−14	0.19	−13	34	−9	0.24	10.24	0.227
	right med. Fronto-orbital gyrus	1	32	−12	0.17	11	25	−14	0.31	12.36	0.218
etc.	19.left Caudate nucleus	−14	4	12	0.28	−16	4	14	0.29	2.83	0.724
	right Caudate nucleus	11	6	12	0.30	13	6	15	0.31	3.61	0.731
	20.left Globus pallidus	−19	−8	1	0.30	−19	−6	1	0.29	2.00	0.612
	right Globus pallidus	17	−7	0	0.28	16	−4	2	0.21	3.74	0.652
	21.left Putamen	−27	−3	3	0.42	−25	−1	1	0.33	3.46	0.663
	right Putamen	−27	−3	3	0.42	24	0	5	0.28	11.12	0.871
	22.left Cingulate	−4	12	32	0.27	−8	−35	43	0.36	48.44	0.168
	right Cingulate	2	21	28	0.27	4	−28	44	0.27	51.58	0.184
	23.left Thalamus	−12	−23	11	0.60	−12	−24	6	0.38	5.10	0.633
	right Thalamus	10	−21	11	0.53	9	−23	8	0.40	3.74	0.71

V. Discussion

1. Construction of Korean Probabilistic Atlas

We have presented the implementation of a group-specific label-based probabilistic atlas and its application method for group analysis. The probabilistic atlas construction method was based on that previously reported by Evans et al. [Evans et al. 1994]. Some steps, such as a standard -space construction method and a manual labeling method in the construction pipeline were optimized in this report. A standard space for the Korean population was constructed to provide a more objective result in spatial normalization and automatic labeling.

In the manual delineation step, we delineated more detailed regions in the cortex. For example, a middle temporal gyrus defined in the MNI probabilistic atlaswas divided into three parts: rostral, intermediate, and caudal. These characteristics allow more detailed analysis in functional imaging studies, such as positron emission tomography (PET) or single photon emission computed tomography (SPECT), where the activated results are mostly of the gray matter. It also offers the advantage of defining the ROIs objectively and indicating the anatomic naming of the ROIs in three-dimensional image data. This approach was first used to quantify the normal range and the distribution of glucose uptake on F-18 fluorodeoxyglucose (FDG)PET [Kang et al., 2001]. Normal ranges for the asymmetric indices of the six gyri of the temporal lobes were established, which were used successfully to identify the gyri of the abnormal range beyond a few deviations in the normal population. Following this report, several investigations into epilepsy have demonstrated the utility of this approach [Lee et al., 2001; Kim et al., 2001; Lee et al., 2002; Kang et al., 2003].

Although manual segmentations of all the atlas structures on all subjects should be used, we used an automatic procedure to segment datasets into anatomical ROIs due to time constraints and inter- or intra-rater variability. The advantages of automatic labeling have been reported previously [Hammers et al., 2002 Hammers et al., 2003]. It is our experience that even a trained observer needs approximately 72 hours to delineate manually all the ROIs to sample the entire volume of a brain. In contrast, the nonlinear registration undertaken in this study takes less than eight hours. The accuracy of nonlinear registration affects the efficiency of anatomic labeling. Although 18 points, which were used for assessment of registration process, were not enough to quantify the registration result, their uniformly distributed positions could be used to estimate the accuracy.

However, the result (1.83 ± 1.55mm of the Euclidean distance) was acceptable considering that the resolution of the functional image was greater than 2 mm. As we used a correction method for improving the labeling quality, mislabeled non-gray-matter voxels were removed and nonlabeled gray-matter voxels were corrected. This scheme is similar to aprevious method reported by Collins [Collins et al., 1999]. We did not perform any quantitative evaluation between the two methods, but this could be pursued in future research. This type of postprocessing for labeling error correction can provide amore efficient result for probabilistic encoding.

2. Group Comparison Study using Probabilistic Atlases

Label-based probabilistic atlases for specific groups contain regional anatomical variability information thatcan characterize group-specific features. From this point of view, it is hypothesized that comparing two probabilistic atlases from different populations may reflect the group-specific differences.

Initial steps for the comparison study were standard-space normalization and ROI matching. For the standard-space matching procedure, the nonlinear transformation method was applied for precise spatial normalization of the two atlases. Each standard space was defined in the form of

an average atlas, which can be more reasonable for performing precise group comparison studies compared to applying the affine transformation method. Alternatively, although it seems more reasonable to define the common standard space for constructing probabilistic atlases, it also has the risk of reducing the accuracy of group-specific probabilistic information. After spatial normalization, ROI matching was included in the procedure for the second preprocessing step. As differences in the ROI delineation produce a reduction of statistical power in the comparison study, it becomes a most critical point for dealing with the confidence of the comparison result. The limitations of the ROI matching procedure are founded in three pairs of ROIs in each hemisphere. These limitations are caused by quite different anatomical landmarks and boundary definitions for ROI delineation. Although this matching has a limitation for perfect recovery of statistical power, it can be a complementary technique in this case.

In the main evaluation procedure, three evaluation factors were used to compare two populations. As each voxel in the ROI contains variability information, the probabilistic volume counting method provides the macroscopic variability information of each ROI. This is due to quite simple concepts. From the nature of a label-based probabilistic atlas, a larger

volume in the low probability threshold means there is a high degree of variability, and a larger volume in the high threshold means that the ROI has a low degree of variability. The degree of variability for each ROI was defined using probabilistic volume counting to compare these variables between two groups. For attaining spatial locating differences, we also defined the probabilistic center of mass for each ROI and measured the Euclidean distances of two corresponding center-of-mass points. Finally, the correlation coefficient for each corresponding ROI provides composite information of two previous factors. The results show that the difference in the degree of variability on the left middle temporal gyrus, left/right postcentral gyrus, right superior temporal gyrus and left/right supra-marginal gyrus, affects the low correlation coefficients. On the other side, the speciallocating difference in the superior frontal gyrus gives the low correlation. This result indicates that differences in regional variability between two different ethnic groups are not homogeneously distributed over the whole brain. This agrees with an earlier report on ethnic difference [Zilles et al. 2001]. The major advantage compared to previous reports is that our method can provide detailed regional differences. Additionally, if the consistency in the atlas construction is guaranteed, our method can be more powerful as a group difference evaluation tool.

Overall, our proposed method could provide a simple but intuitive ROI-based group analysis of the entire cortex area. The regions relating to group-specific variation factors such as genetics, age and disease, could be classified without complicated high-order statistics. From this point of view, our method could be used as a prompting system to highlight regions of the brain worthy of further analysis by various subcortical region-based group studies in assessing specific patterns related to diseases. In the future, studies on age-and sex-related regions for the Korean normal group will be assessed from subpopulation atlases using the same procedure.

VI. Acknowledgement

References

[1]   Ashburner J, Friston KJ (1997): Multimodal image coregistration and partitioning: a unified framework.Neuroimage 6: 209-217.

[2] Bajcsy R, Lieberson R, Reivich M (1983): A computerized system for the elastic matching of deformed radiographic images to idealized atlas images. J Comput Assist Tomogr 7: 618–625.

[3] Bohm C, Greitz T, Kingsley D, Berggren BM, Olsson L (1983): Adjustable computerized stereotaxic brain atlas for transmission and emission tomography. Am. J. Neuroradiol. 4: 731–733.

[4] Christensen GE, Joshi SC, Miller MI (1997): Volumetric transformation of brain anatomy. IEEE Trans. Med. Imaging 16: 864–877.

[5] Collins DL, Zijdenbos AP, Baare WFC, Evans AC (1999): ANIMAL+INSECT: Improved cortical structure segmentation. Lect. Notes Comput. Sc. 1613: 210–223.

[6] Crespo-Facorro B, Kim JJ, Andreasen NC, O'Leary DS, Wiser AK, Bailey JM, Harris G, Magnotta VA (1999): Human frontal cortex: an MRI-based parcellation method. Neuroimage 10: 500–519.

[7] Crespo-Facorro B, Kim JJ, Andreasen NC, Spinks R, O'Leary DS, Bockolt HJ, Harris G, Magnotta VA (2000): Cerebral cortex: a topographic segmentation method using magnetic resonance imaging. Psychiatry Res. Neuroim. 100: 97–126.

[8] Evans AC, Beil C, Marrett S, Thompson CJ, Hakim A (1988): Anatomical-functional correlation using an adjustable MRI-based region of interest atlas with positron emission tomography. J. Cereb. Blood Flow Metab. 8: 513–530.

[9] Evans AC, Collins DL, Milner B (1992): An MRI-based stereotactic brain atlas from 300 young normal subjects. Proc. 22nd Annu. Symp. Soc. Neurosci. 408.

[10] Evans AC, Kamber M, Collins DL, MacDonald D (1994): An MRI-based probabilistic atlas of neuroanatomy. In: Shorvon SD, Fish DR, Andermann F, Bydder GM, Stefan H, editors. Magnetic resonance scanning and epilepsy. New York: Plenum Press. p 263–274.

[11] Greitz T, Bohm C, Holte S, Eriksson L (1991): A computerized brain atlas: Construction, anatomical content, and some applications. J. Comput. Assist. Tomogr. 15: 26–38.

[12] Hammers A, Allom R, Koepp MJ, Free SL, Myers R, Memieux L, Mitchell TN, Brooks DJ, Duncan JS (2003): Three-dimensional maximum probability atlas of the human brain, with particular reference to the temporal lobe. Hum. Brain Mapp. 19:224–247.

[13] Hammers A, Koepp MJ, Free SL, Brett M, Richardson MP, Labbé C, Cunningham VJ, Brooks DJ, Duncan J (2002): Implementation and application of a brain template for multiple volumes of interest. Hum. Brain Mapp. 15: 165–174.

[14] Kang E, Lee DS, Lee JS, Kang H, Hwang CH, Oh SH, Kim CS, Cung JK, Lee MC, Jang MJ, Lee YJ, Morosan P,

Zilles K (2003): Developmental hemispheric asymmetry of interregional metabolic correlation of the auditory cortex in deaf subjects. Neuroimage 19: 777‒783.

[15] Kang KW, Lee DS, Cho JH, Lee JS, Yeo JS, Lee SK, Chung JK, Lee MC (2001): Quantification of F-18 FDG PET images in temporal lobe epilepsy patients using probabilistic brain atlas. Neuroimage 14: 1‒6.

[16] Kabani NJ (1998): A 3D neuroanatomical atlas of the Human Brain. Neuroimage 7(4), pt. 2.

[17] Kim JJ, Crespo-Facorro B, Andreasen NC, O'Leary DS, Zhang B, Harris G, Magnotta VA (2000): An MRI-based parcellation method for the temporal lobe. Neuroimage 11: 271‒288.

[18] Kim JS, Lee JM, Lee YH, Kim JS, Kim IY, Kim SI (2002): Intensity based affine registration including feature similarity for spatial normalization. Comput. Biol. Med. 32: 389‒402.

[19] Kim JS, Lee JM, Kim JJ, Choe BY, Oh CH, Kwon JS, Kim SI (2003): Non-linear registration for brain images by maximizing feature and intensity similarities with a Bayesian framework. Med. Biol. Eng. Comput. 41: 473‒480.

[20] Kim SK, Lee DS, Lee SK, Kim YK, Kang KW, Chung CK, Chung JK, Lee MC (2001): Diagnostic performance of [18F]FDG-PET and ictal [99mTc]-HMPAO SPECT in occipital lobe epilepsy. Epilepsia 42: 1531‒1540.

[21] Kosugi Y, Sase M, Kuwatani H, Kinoshita N, Momose T, Nishikawa J, Watanabe T (1993): Neural network mapping for nonlinear stereotactic normalization of brain MR images. J. Comput. Assist. Tomogr. 17: 455‒460.

[22] Lee DS, Lee JS, Kang KW, Jang MJ, Lee SK, Chung JK, Lee MC (2001): Disparity of perfusion and glucose metabolism of epileptogenic zones in temporal lobe epilepsy demonstrated by SPM/SPAM analysis on ^{15}O water PET, [^{18}F] FDG-PET, and [^{99m}Tc]-HMPAO SPECT. Epilepsia 42: 1515‒1522.

[23] Lee JM, Koo BB, Lee SM, Kim IY, Kim SI (2003): A Novel Automatic Algorithm for Selecting a Standard Brain in a Data Set using Simple Structure Analysis in Talairach Coordinate System. Journal of digital imaging, 16(1) suppl.: 95‒96

[24] Lee SK, Lee DS, Yeo JS, Lee JS, Kim YK, Jang MJ, Kim KK, Kim SK, Oh JB, Chung CK (2002): FDG-PET images quantified by probabilistic atlas of brain and surgical prognosis of temporal lobe epilepsy. Epilepsia 43: 1032‒1038.

[25] Talairach J, Tournoux P. 1988. Co-planar stereotaxic atlas of the human brain. New York: Georg Thieme Verlag.

[26] Thompson PM, Woods RP, Mega MS, Toga AW (2000): Mathematical/computational challenges in creating deformable and probabilistic atlases on

the human brain. Human Brain Mapping 9: 81-92.

[27] Yoon UC, Lee JM, Kim JJ, Kim IY, Kwon JS, Kim SI (2003): Modified MRI-Based Parcellation Method for Cerebral Cortex using Successive Fuzzy Clustering and Boundary Detection. Ann. Biomed. Eng. 31: 441-447.

[28] Zilles K, Kawashima R, Dabringhaus A, Fukuda H, Schormann T (2001): Hemispheric Shape of European and Japanese Brains: 3-D MRI Analysis of Intersubject Variability, Ethnical, and Gender Differences. Neuroimage 13: 262-271.

저자소개

구 방 본

2002년 2월 한양대학교 응용물리학 전공
2004년 2월 한양대학교 의용생체공학 석사
2008년 8월 한양대학교 의용생체공학 박사
2008년 10월~현재 Research Fellow, Multi-modal Whole Animal Imaging Core, National Emerging Infectious Disease Laboratory (NEIDL), Boston University Medical Center

주관심 분야 : Multimodal Bio-Imaging(3D optical imaging, MRI, CT, Ultrasound), Computational Neuro-anatomy

이 종 민

1999년 2월 서울대학교 의용생체공학과 박사
1994년 2월 서울대학교 의용생체공학과 석사
1992년 2월 서울대학교 공과대학 제어계측공학과 학사
2005년 3월~현재 한양대학교 공과대학 전기생체공학부 생체공학전공 조교수/부교수
2001년 3월~2005년 2월 한양대학교 의과대학 의공학교실 연구교수/조교수
2000년 3월~2001년 2월 메디다스 부설연구소 선임연구원
1999년 3월~2000년 2월 대우전자 연구소 선임연구원

주관심 분야 : 뇌영상처리, 전산신경과학, 의학영상처리